Two-dimensional *XY* and clock models studied via the dynamics generated by rough surfaces

A. Faissal Brito,[1,2] José Arnaldo Redinz,[3] and J. A. Plascak[1,4]

[1]*Departamento de Física, Instituto de Ciências Exatas, Universidade Federal de Minas Gerais, C.P. 702, 30123-970, Belo Horizonte, MG, Brazil*

[2]*Instituto de Ciências Exatas, Humanas e Sociais Aplicadas–ICEHSA, Centro Universitário de Caratinga–UNEC, Campus de Nanuque, 39860-000 Nanuque, MG, Brazil*

[3]*Departamento de Física, Universidade Federal de Viçosa, 36570-000 Viçosa, MG, Brazil*

[4]*Department of Physics and Astronomy, University of Georgia, 30602 Athens, Georgia, USA*

(Received 12 February 2010; published 29 March 2010)

The p-state clock model is studied, for general values of p, from simulations using a heat-bath single spin flipping Monte Carlo method, and a mapping of the corresponding spinlike configurations to a solid-on-solid growth model. The growth exponents are calculated. From the dynamics generated by this far from equilibrium kinetic roughening of the surface one is able to characterize the corresponding equilibrium magnetic properties of the original model, such as the high temperature Berezinskii-Koserlitz-Thouless (BKT) transitions, the low-temperature long-range ordered phase transitions, as well as the conventional second-order phase transitions. The present method suggests that for $p \geq 5$ the high-temperature phase transition is indeed a BKT one, whose value is the same as that for $p \to \infty$ (XY model), while the low-temperature phase transition has a first-order character.

DOI: 10.1103/PhysRevE.81.031130 PACS number(s): 05.50.+q, 02.50.−r, 68.35.Ct, 68.35.Rh

I. INTRODUCTION

Much attention has been recently given to the study of the p-state clock model (see, for instance [1–3], and references therein). For $p=2$, 4, and 3 one has the Ising and three-state Potts model, respectively, and in the limit as the number of states goes to infinity it corresponds to the XY (planar rotator) model. While the Ising and three-state Potts models present a conventional continuous critical behavior, the latter one exhibits the peculiar and exotic Berezinskii-Kosterlitz-Thouless (BKT) transition [4]. Thus, the p-state clock system is interesting not only because it is an interpolation between the Ising and Potts universality classes on one side and, on the other side, the BKT transition [4,5], but because it also presents the called *extended universality* at some p-dependent temperature region the thermodynamic variables (such as energy, magnetization, susceptibility, etc.) are still identical [1].

Elitzur *et al.* [5], using a renormalization group procedure, have shown that there is a critical value p_c, above which an intermediate XY-like phase appears. This is in contrast of what one would expect, namely an Ising like continuous transition for finite p, with the BKT transition only in the limit $p \to \infty$. More specifically, for $p=2$ and 4 the system is equivalent to the Ising model, and for $p=3$ it is equivalent to the three-states Potts model. In these cases, one has a low-temperature ordered phase and a high-temperature disordered phase with a conventional continuous phase transition line separating them. The same holds for $4 < p < \infty$, however, in this range there is a quasiliquid (XY-like) intermediate phase with two transition temperatures $T_2 > T_1$, where T_1 is the transition from the ordered phase to the quasiliquid phase and T_2 the transition from the latter one to the disordered phase.

Recently, Lapilli *et al.* [1], using Monte Carlo simulations, have shown that the model also presents *extended universality*. This means that for some temperature $T > T_{eu}(p)$, not only the critical exponents are the same, but indeed all thermodynamic variables are identical.

Although what has been said above is quite general and in agreement with several approximate techniques, there are still controversies regarding some details of the global phase diagram when one looks at the transition temperature as a function of the number of states p. (i) the first question concerns the value of p_c, at which for $p < p_c$ there is only one conventional transition temperature. Elitzur *et al.* [5] estimated $p_c=4$ and Roomany and Wyld [6], by using finite-lattice method, obtained $p_c=5$. Monte Carlo renormalization group procedure of Tobochnik [7] have shown that $p_c=4$. (ii) previous works show that for $p > p_c$ both transitions T_2 and T_1 are of BKT type. On the other hand, recent Monte Carlo results by Lapilli *et al.* [1] indicate that only for $p \geq 8$ the transition at T_2 is of BKT type, while T_1, for all finite p, differs from BKT; (iii) the behavior at $p=5$ is still inconclusive.

In one of the main goals in this work we address to the question of the phase diagram, in the temperature versus number of states plane, of the clock model (for general values of p) by using Monte Carlo simulations. We have analyzed the two-dimensional surface generated by its spinlike configurations according to a procedure recently proposed by Brito *et al.* [8], which consists of generating a surface from the corresponding spinlike configurations obtained from usual Monte Carlo simulations. The configurations are mapped onto a solid-on-solid growth model. The dynamic growth of the surface, at a given temperature, is then studied and from the respective roughness and the corresponding rough exponents one is able to get insight of the first order and continuous phase transition lines, as well as multicritical points. In particular, one is interested here in obtaining the roughness α, and the growth β_w exponents [9–11]. The method has been successfully applied to the Ising, Blume-Capel, and Potts models [8]. Not only good results have been

achieved regarding the order of the transition, but also growth exponents have been obtained from such surface dynamics. This dynamic surface generating method in treating critical properties of magnetic models is completely different from standard Monte Carlo simulations. In the present case, one does not compute the equilibrium magnetic thermodynamic variables to get the properties of system, but the corresponding scaling behavior of the mapped solid-on-solid far from equilibrium rough surface instead.

Moreover, the present work is in fact twofold. First, treating the general properties of the clock model, where there are still some open questions regarding its phase diagram. Second, applying for the first time the solid-on-solid generating surface approach to a continuous spin system, namely the two-dimensional XY model (planar rotator model). In this sense, we will also be interested in obtaining the dynamic critical behavior of their growth surfaces and determining their corresponding universality classes. From a theoretical point of view this is, by itself, important in what concerns the dependence of the critical exponents on the dimensionality.

The plan of the paper is as follow. In Sec. II we present the model and the simulation details. In Sec. III we discuss the corresponding generating surface approach. The transition temperatures and the global phase diagram as a function of the number of states p are presented in Sec. IV, while in Sec. V we present the surface exponents and the finite-size scaling relation for the roughness. Section VI is devoted to the concluding remarks.

II. MODEL AND SIMULATIONS

A. Model

The p-state clock model can be defined by the following Hamiltonian

$$\mathcal{H} = -J\sum_{\langle i,j\rangle} \cos(\theta_i - \theta_j), \tag{1}$$

where $\theta_i=(2\pi/p)\sigma_i$ is the angle that the spinlike variable of unitary length S_i makes with an arbitrary axis and each spin variable S_i assumes p different orientation states given by $\sigma_i=0,1,2,\ldots,p-1$. J is the exchange interaction, assumed to be ferromagnetic $J>0$, and the sum is over nearest-neighbor pairs of sites on a two-dimensional square lattice.

For $p=2$, the spins are either parallel ($\sigma_i=0$ and spin $S_i=1$) or antiparallel ($\sigma_i=1$ and spin $S_i=-1$) to the arbitrary axis. This makes the Hamiltonian (1) exactly the same as the spin-1/2 Ising model $\mathcal{H}=-J\Sigma_{\langle i,j\rangle}S_iS_j$, with the critical temperature $k_BT_c^{p=2}/J=p/\ln(\sqrt{p}+1)$, where k_B is the Boltzmann constant. On the other hand, as $\cos(2\pi/3)=\cos(4\pi/3)$ we get, for $p=3$, $\mathcal{H}=-J[1-\cos(2\pi/3)]\Sigma_{\langle i,j\rangle}\delta_{\sigma_i\sigma_j}$, where $\delta_{\sigma_i\sigma_j}$ is the Kronecker delta. This Hamiltonian is equivalent to the three-state Potts model with $k_BT_c^{p=3}/J=1.5/\ln(\sqrt{p}+1)$. Moreover, due to the fact that $\cos(\pi/2)=\cos(3\pi/2)=0$ one gets for $p=4$ two independent spin-1/2 Ising models and $k_BT_c^{p=4}/J=k_BT_c^{p=2}/2J$. For $p>4$ no exact solution is available and two transitions take place for values of p greater than a critical value p_c.

B. Simulations

The Monte Carlo (MC) simulations of the model given by Eq. (1) have been performed on square lattices with $N=L\times L$ sites submitted to periodic boundary conditions. For updating the spin configurations $\{\sigma_i(t)\}$, where $\{\sigma_i(t)\}=\{\sigma_1(t),\sigma_2(t),\ldots,\sigma_N(t)\}$, we used a single spin-flip Monte Carlo heat-bath algorithm, with the update being performed sequentially through the whole lattice.

The corresponding surface growth process, which is the same as that described by Brito *et al.* in Ref. [8], consists in accumulating, i.e., summing up all the values assumed by the spin variables $\sigma_i(t)$ over the first t Monte Carlo time steps. Specifically, to an unique sequence of spin variable states $(\{\sigma_i(0)\},\{\sigma_i(1)\},\ldots,\{\sigma_i(t)\})$ corresponds a surface $\{h_i(t)\}$ with the height $h_i(t)$ at site i and time t given by

$$h_i(t) \equiv \sum_{t'=0}^{t} \rho_i(t'). \tag{2}$$

In the above expression we have: (i) $\rho_i(t')=+1$ or -1 when $\sigma_i(t')=0$ or 1, as for the $p=2$ model; (ii) $\rho_i(t')=+1$, 0, or -1 when $\sigma_i(t')=0$, 1, or 2, as for the $p=3$ model; (iii) and so on for higher values of p; (iv) $\rho_i(t')=\cos(\theta_i)$ for the planar rotator model when $p\to\infty$ (in this case, due to the symmetry in the plane interactions, $\rho_i(t')=\sin(\theta_i)$ could also be considered).

The model (2) defines a process of the solid-on-solid-like type, resulting in an aggregate which is compact (no vacancies) and free of surface overhangs. It can be seen that the interface so generated advances in time by deposition ($\rho_i>0$) and evaporation ($\rho_i<0$) of atoms on the initial substrate. In the low-temperature phases of the spin models we expect that the deposition processes dominate and the interface average height increases with time. At high temperatures, the two processes, deposition and evaporation, take place with equal probability and the velocity of the interface growing goes to zero. Thus, the surface $\{h_i(t)\}$ can be thought of as a driven interface whose dynamics, as we will see below, reflects the critical, BKT or first-order properties of the models.

Our simulations have been performed with initial configurations in which all the spins were ordered in the larger spin value ($\{\sigma_i(0)=p-1\}$) and the initial deposit substrate was flat ($\{h_i(0)=0\}$). Although the final results are independent of this initial condition, it is closer to the flat substrate condition employed in most surface growth simulations. The linear system size in the simulations was changed between $L=32$ and $L=160$. The maximum Monte Carlo time ranged from about $t=10^2$ (where only short times were needed) to $t=10^6$. To obtain good statistics we took averages over 100–2000 independent runs, depending on the p-state model, the temperature, the system size, and the time regime of the measurements.

III. SURFACE FORMALISM

In order to get the basic scaling analysis of the growing surface, one can characterize the development of the fluctuations of the two-dimensional interface, with heights $h_i(t)$ for

the site i at time t, over a window of linear size ϵ by the root-mean-square displacement function, or local roughness, $W(\epsilon,t)$ given by

$$W(\epsilon,t) = \sqrt{\langle \overline{h^2} - \bar{h}^2 \rangle_i}, \tag{3}$$

where the brackets $\langle \ldots \rangle_i$ denote an average over the window position $i=1,2,\ldots,L^2$. The averages $\bar{h}$ and $\overline{h^2}$ are defined through

$$\bar{f} = \frac{1}{\epsilon^2} \sum_{\vec{r}} f(\vec{r}), \tag{4}$$

with the sum over the positions $\vec{r}$ inside a two-dimensional window of linear size ϵ centered at site $\vec{r}_i$.

It is known that at long times this local roughness behaves as [9–11] $W(\epsilon, t \gg t_c) \sim \epsilon^H$, where t_c is a crossover time and H is the Hurst exponent. In this regime, the roughness $W(\epsilon,t)$ can distinguish two possible types of profiles: (i) if it is random, or even exhibits a finite correlation length extending up to a characteristic range (such as in a Markov chain), then $W \sim \epsilon^{1/2}$ with $H=1/2$, as in a normal random walk; (ii) in contrast, if the self-affine profile has infinitely long-range correlations (no characteristic length), then we expect $H \neq 1/2$.

On the other hand, the scaling ansatz for the global roughness, i.e., $W(L,t)=W(\epsilon=L,t)$, with respect to time t and the size L, is given by the Family-Vicsek relation [10,12]

$$W(L,t) \sim L^{\alpha} f\left(\frac{t}{L^{z_w}}\right), \tag{5}$$

where $f(u)$ is a universal scaling function, α is the roughness exponent, $z_w=\alpha/\beta_w$ is the dynamic exponent, and β_w is the growth exponent. Two distinct behaviors are expected for $f(u)$: (i) $f(u)=c$, where c is a constant, at long times ($t \gg t_c, u \gg 1$) and; (ii) $f(u) \sim u^{\beta_w}$ at short times ($t \ll t_c, u \ll 1$). In this way, at short times, we expect $W(t) \sim t^{\beta_w}$. At long times, when the lateral (spatial) correlation length of the growth process equals the lattice length L, the roughness saturates and behaves as $W(L,\infty) \sim L^{\alpha}$. The crossover time t_c between these two regimes grows as $t_c \sim L^{z_w}$. The particular case in which W does not saturate, growing instead as $W(L,t) \sim t^{1/2}$, corresponds to uncorrelated growth. Thus, the exponent α is not defined for this case and $\beta_w=1/2$. Typically, the exponents $H=\beta_w=1/2$ are characteristic of the random deposition (RD) growth model, in which a column is randomly chosen along the substrate and a particle is launched vertically until it is deposited at the top of the selected column. In general, H and α are often most the same thing, in particular when the simple Family-Vicsek scaling applies [10,12].

For models presenting a continuous transition, away from criticality, the correlation length ξ and the correlation time τ of the spin models are finite, and the corresponding noise in the deposition process is correlated only over short ranges. We expect that in this case, for times greater than τ, the noise appears uncorrelated, and that the RD growth exponents, $H=\beta_w=1/2$, are verified from the first steps in the growth process.

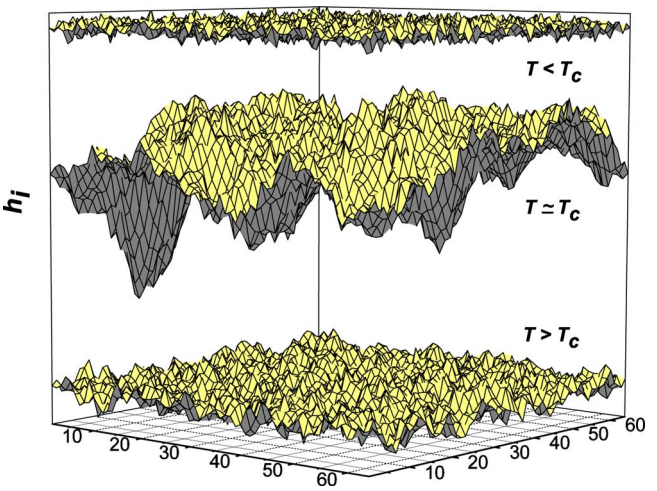

FIG. 1. (Color online) Typical interfaces obtained from equilibrium spin configurations of the $p=2$ clock model (Ising model) on the square lattice with $L=64$ at the temperatures above, below and near T_c (figure from Ref. [8]).

In contrast, at a continuous phase transition, and also at a BKT transition, ξ and τ diverge and the correlations are long ranged, giving a power-law decay of the noise autocorrelation. In this case, the exponents H and β_w should deviate from 1/2.

At a first-order phase transition there is no long-range correlations and we expect again $H=\beta_w=1/2$ even at the transition temperature. However, in cases where the order of the transition is difficult to be distinguished in finite systems, these RD values cannot be attained in the simulations. In the five-states Potts model, for example, there is an apparent divergence of the correlation length in the critical region and pseudocritical exponents can be defined [13].

IV. TRANSITION TEMPERATURES AND GLOBAL PHASE DIAGRAM

For convenience, in what follows, the temperature T will be measured in units of J/k_B.

A. Ising $p=2,4$ and Potts $p=3$ models

For $p=2,4$, and for $p=3$, we get the previous results from Ref. [8] for the spin-1/2 Ising and the three-state Potts models, respectively. As a matter of completeness, we reproduce in Fig. 1 earlier typical snapshots obtained in reference [8] for the surfaces generated by equilibrium spin configurations of the spin-1/2 Ising model (or $p=2$ clock model). We can note that for $T \neq T_c$ the surfaces appear rough down to short length scales, whereas for $T \simeq T_c$ the surface presents large fluctuations. So, the roughness W as a function of temperature presents a maximum around the continuous transition.

From this maximum observed in the roughness W for arbitrary long times and different lattice sizes, we can show that there is an ordered phase at low temperatures and a disordered phase at high temperatures, with a continuous conventional transition at T_c^p. We obtained $T_c^{p=2}=2.266(3)$, $T_c^{p=3}=1.489(7)$, and $T_c^{p=4}=1.133(3)$, which should be com-

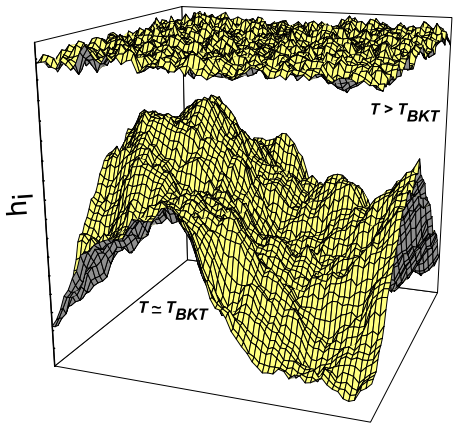

FIG. 2. (Color online) Typical interfaces obtained from equilibrium spin configurations of the planar rotator model on the square lattice with $L=64$ at the temperatures above and near T_{BKT}. For all temperatures $T<T_{BKT}$ the surface is similar to that near T_{BKT}.

pared to the exact results $T_c^{p=2}=2.269$, $T_c^{p=3}=1.492$, and $T_c^{p=4}=1.134$, respectively [note that for $p=3$ and $p=4$ these critical temperatures have been suitably normalized according to what have been discussed above regarding the equivalence of the model given by Eq. (1) and the Ising and Potts ones]. We do not reproduce here these finite size scaling results since they have been already discussed in Ref. [8]. The corresponding surface exponents β_w and H, as well as the dynamic exponent z_w, are also given in [8].

B. Planar rotator model $p \to \infty$

Figure 2 shows some snapshots of the surface generated by the equilibrium spin configurations for the planar rotator model on the square lattice with $L=64$. It is very similar to Fig. 1, except from the fact that for all temperatures $T<T_{BKT}$ the corresponding surfaces present large fluctuations, reflecting the fact that one has a BKT-like phase.

The roughness as a function of temperature for different lattice sizes are depicted in Fig. 3. One can see that the roughness increases as the temperature decreases, reaching a peak at $T_{BKT}(L)$, which is size dependent, and for $T<T_{BKT}(L)$ it stays quite large down to low temperatures, indicating the presence of the BKT phase.

As the planar rotator model is in the same universality class of the XY model, the correlation length ξ is expected to behave as [14]

$$\xi = \exp\left(\frac{B}{\sqrt{T_{BKT}(L) - T_{BKT}}}\right). \tag{6}$$

Thus, for a finite lattice of linear size L one has, close to the BKT transition, $\xi \sim L$, from where we get

$$T_{BKT}(L) = T_{BKT} + \frac{C}{(\ln L)^2}, \tag{7}$$

with $T_{BKT}(L)$ being the estimated transition temperature for the finite lattice L, T_{BKT} being the transition temperature in the thermodynamic limit, and B e C nonuniversal constants. The finite-size scaling of the data obtained from Fig. 3 is

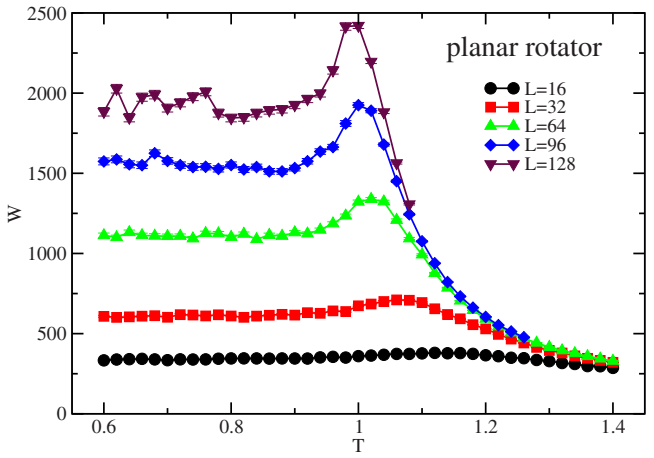

FIG. 3. (Color online) Roughness W as a function of the reduced temperature T for the planar rotator model and several values of linear lattice sizes L. The simulation time is $t=2\times10^4$ MCS and the averages were taken over 1000 independent runs. The full lines are just guide to the eyes and the error bars are smaller than the symbol sizes.

shown in Fig. 4, from which we obtain $T_{BKT}=0.89(1)$, which is comparable to the values from the literature [1,15]. Notice that in this case we have to consider the bigger lattices in order to get a reasonable finite-size behavior.

In the previous work [8] only the roughness has been used to get the transition temperature of the system. However, we can still exploit the behavior of the growth exponent β_w. In this case, since it is obtained from the short-time behavior of the growing surface, we can resort to a better statistics. Figure 5 shows the growth exponent as a function of the temperature for different lattice sizes. For high-temperatures β_w approaches the value 1/2, as expected for random deposition since in this case there is no correlation in the magnetic system. As temperature decreases, however, the magnetic

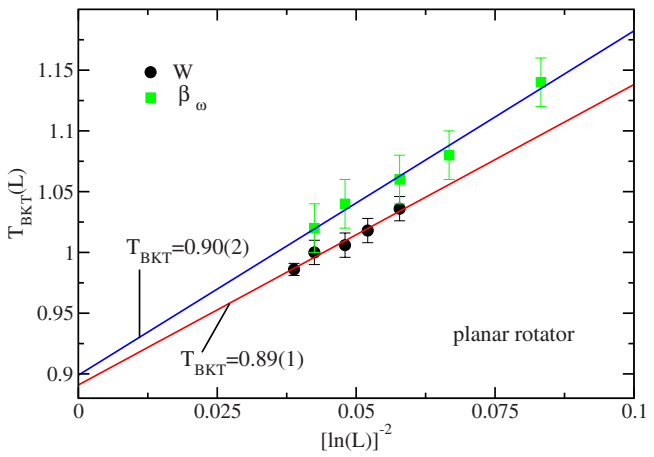

FIG. 4. (Color online) Finite size scaling of the temperature peak for the planar rotator model for several values of linear lattice sizes. From the roughness W one has $L=64,80,96,128,160$, with the simulation time of $t=2\times10^4$ MCS and the averages taken over 1000 independent runs. From the β_w exponent one has $t=200$ MCS and averages over 10^4 samples with $L=32,48,64,96,128$. The full lines are the best fits according to Eq. (7).

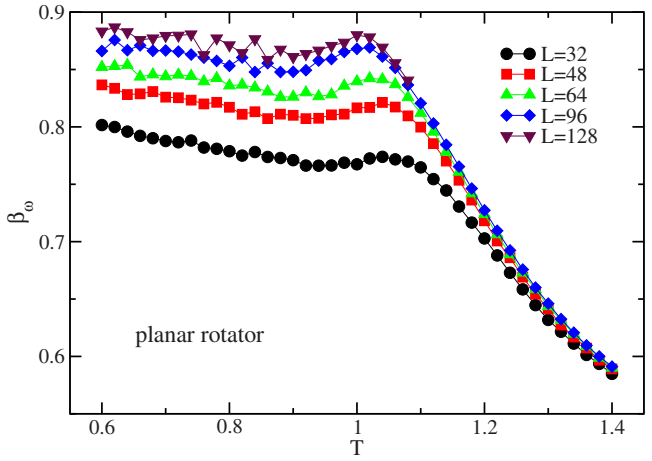

FIG. 5. (Color online) Growth exponent β_w as a function of the reduced temperature T for the planar rotator model and several values of linear lattice sizes L. The simulation time is $t=200$ MCS and the averages were taken over 10^4 independent runs. The full lines are just guide to the eyes and the error bars are smaller than the symbol sizes.

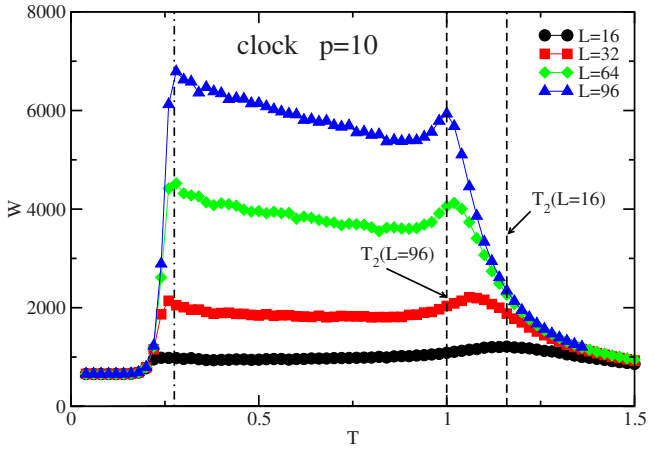

FIG. 6. (Color online) Roughness W as a function of the reduced temperature T for the $p=10$ clock model and several values of linear lattice sizes L. The simulation time is $t=2\times10^4$ MCS and the averages were taken over 2000 independent runs. The vertical dashed lines locate the transition temperature T_2 for different lattice sizes and the vertical dot-dashed line locates the transition temperature T_1. The full lines are just guide to the eyes.

system becomes highly correlated and the growth exponent becomes different from 1/2 at the BKT transition. The fact that this exponent stays almost constant for even lower temperatures indicates a highly correlated state in this region, which reflects the presence of the BKT phase for $T<T_{BKT}$. It is also apparent from Fig. 5 that the peak of the growth exponent is size dependent. The corresponding finite size scaling of $T_{BKT}(L)$ obtained from β_w is also depicted in Fig. 4, where one gets $T_{BKT}=0.90(2)$, which is, within the error bars, comparable to that obtained from the roughness W and from other values in the literature [1,15]. In addition, one can note that the present approach, based on the analysis of the nonequilibrium properties of growing surfaces, is also able to get the BKT transition for continuous spin models. We also expect that the present method should still be useful in studying classical continuous spin models undergoing conventional second-order transitions.

C. $5<p<\infty$

For these models one has two distinct transition temperatures, namely, a high temperature T_2 from the disordered phase to the BKT-like phase (also called spin wave phase) and a lower temperature from the spin wave phase to the ordered phase.

1. Temperature T_2

Figure 6 shows the roughness as a function of temperature for the $p=10$ clock model and different lattice sizes. There is a kind of plateau, where the roughness increases with the system size, analogously as it occurs in the critical points of the $p\leq4$ models and in the low-temperature phase of the *XY* model. One can also note that out of the plateau region the roughness is small and independent of the system size. This is an indication that the magnetic system should be highly correlated for temperatures $T_1<T<T_2$, as is expected in the spin-wave phase. Such behavior will also be noticed in the growth exponent discussed below. Thus, in what follows, this phase will be associated with this range of temperatures. We observe that the higher transition temperature $T_2(L)$ is lattice size dependent, whereas the lower one T_1 is almost independent on L, mainly for the larger lattices.

In Fig. 7, we show the roughness as a function of temperature for the lattice size $L=32$ and several values of the clock states p. For $4<p<10$ we clearly see two temperatures, where in this case T_1 varies with p and T_2 is almost independent of p, even for this small lattice. Just as a matter of comparison, it is also shown the temperature T_1 obtained

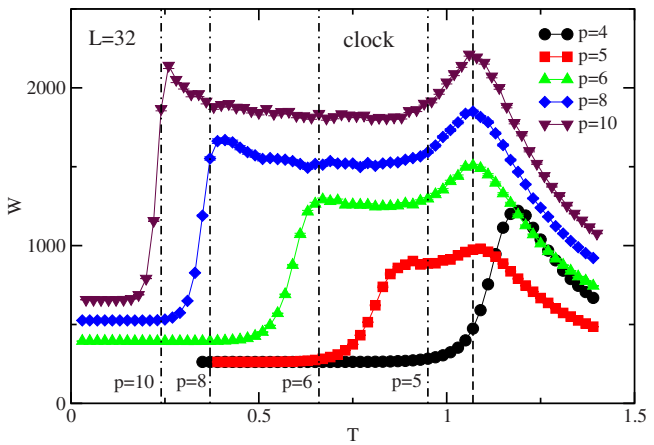

FIG. 7. (Color online) Roughness W as a function of the reduced temperature T for the p-state clock model and several values of p and linear lattice size $L=32$. The simulation time is $t=2\times10^4$ MCS and the averages were taken over 2000 independent runs. The vertical dashed line locates the transition temperature T_2, and the dot-dashed lines locate the transition temperature T_1, for different values of p, according to Ref. [1]. The full lines are just guide to the eyes.

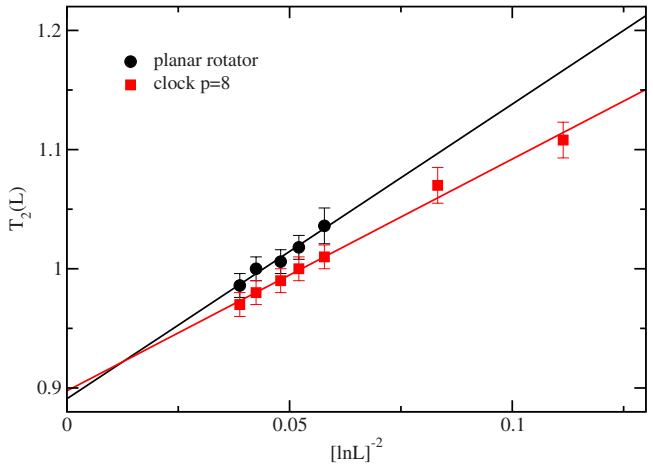

FIG. 8. (Color online) Finite-size scaling of the temperature $T_2(L)$ obtained from the roughness W for the $p=8$ clock model. The lattice sizes are $L=20,32,64,80,96,128,160$. For comparison, we also have the previous results for the planar rotator model and $L=64,80,96,128,160$. The lines are the best fits according to Eq. (7).

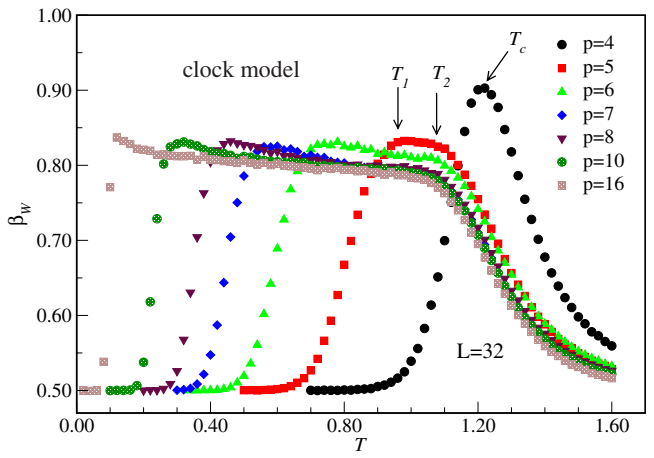

FIG. 9. (Color online) Growth exponent β_w as a function of the reduced temperature T for the clock model with $L=32$ and several values of p. The simulation time is $t=200$ MCS and the averages were taken over 10^4 independent runs. The error bars are smaller than the symbol sizes.

in reference [1], from which one sees a good agreement even for small lattice $L=32$. For $p=5$ one can note two distinct temperatures, however, as we will see below, a finite-size scaling of T_2 leads to just one transition for this model. For $p=4$, as expected, only one peak is observed, characterizing the continuous order-disorder phase transition.

As an example, a finite-size scaling of $T_2(L)$, coming from the behavior of the roughness as a function of the temperature, is shown in Fig. 8 for the case $p=8$. We get, in this case, $T_2^{p=8}=0.898(7)$ and should be compared to $T_{BKT}=0.89(1)$ for the planar rotator model which is also shown in Fig. 8 for comparison. Similarly, we can obtain T_2, in the thermodynamic limit, for other values of p. In this case, within the error bars, the transition temperatures are comparable to the T_{BKT} obtained in the limit $p\to\infty$.

We can also resort to the behavior of the growth exponent as a function of temperature. Some results are depicted in Fig. 9 for several values of the model states and lattice size $L=32$. Except for $p=4$, where we have only an order-disorder continuous transition, one can note that for $T_1<T<T_2$ (where the lower temperature T_1 is clearly p dependent) the growth exponent is different from 1/2, indicating the presence of a spin-wave phase, while for temperatures out of this interval the exponent is 1/2, typical of uncorrelated systems. Despite T_1 being well defined for this lattice size, the higher transition temperature T_2 is not so well defined as the corresponding behavior of the roughness shown in Fig. 7. However, even in this case, a coarse finite-size scaling of T_2 leads, within the error bars, to the same results as those from the roughness W shown in Fig. 8.

2. Temperature T_1

Figure 6 shows that for a fixed value of p the temperature T_1 is almost lattice independent. The same behavior we get from the growth exponent β_w (not shown). Figure 10 depicts the estimates of T_1 as a function of the lattice size from two different clock states from where we see that T_1 is almost constant. Similar results are obtained for other values of p. It is also interesting to plot T_1 as a function of $1/p^2$ as is shown in Fig. 11. From these plots one gets $T_{1\beta}=0.03(2)+25(1)/p^2$ from the β_w exponent and $T_W=0.02(2)+24(1)/p^2$ from the roughness behavior, which are comparable to $T_1=23.4/p^2$ reported in Ref. [1]. One can note that there is a difference in T_1 coming from W and β_w for small values of p (in what follows the estimate of T_1 is the average from both measurements).

3. p=5 clock model

Let us analyze now the particular case $p=5$ where there is no convincing result yet in the literature. As discussed above, it is more convenient to consider the roughness as a function of the temperature since with this quantity the resolution of

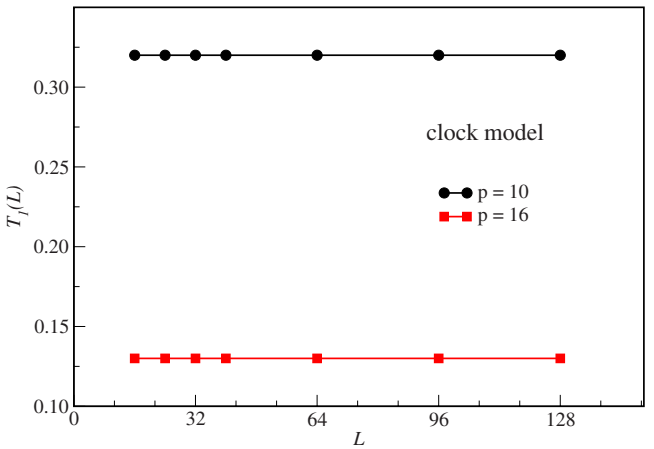

FIG. 10. (Color online) Finite-size dependence of the temperature $T_1(L)$ obtained from the growth exponent β_w for the $p=10$ and 16 clock models. From the β_w exponent one has $t=200$ MCS and averages over 10^4 samples. The error bars are smaller than the symbol sizes.

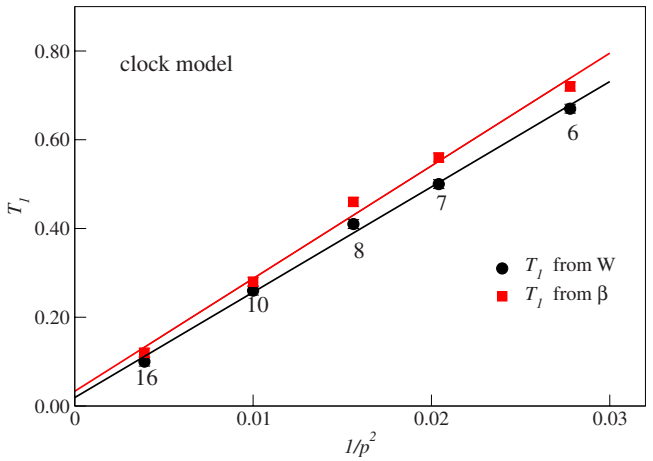

FIG. 11. (Color online) Temperature T_1 as a function of $1/p^2$ obtained from the growth exponent β_w and from the roughness W for different clock state models (indicated in the figure). For the β_w exponent one has $t=200$ MCS and averages over 10^4 samples, while for W one has $t=2\times10^4$ MCS and the averages were taken over 2000 independent runs. The error bars are smaller than the symbol sizes.

T_2 is better (although the required MC time is longer). In Fig. 12 we have the roughness W as a function of T for $p=5$ and different lattice sizes. As for the other models, T_1 is almost independent of the lattice sizes whereas T_2 has a strong dependence on L. The lower transition is estimated to be $T_1=0.91(2)$. The finite size scaling of $T_2(L)$ is shown in Fig. 13. From a fit with Eq. (7) one gets $T_2^{p=5}=0.90(2)$ which is comparable, within the error bars, to T_1 and T_{BKT}. Thus, in this case, from the present method one gets, within the error bars, the same BKT transition temperature for the $p=5$ model.

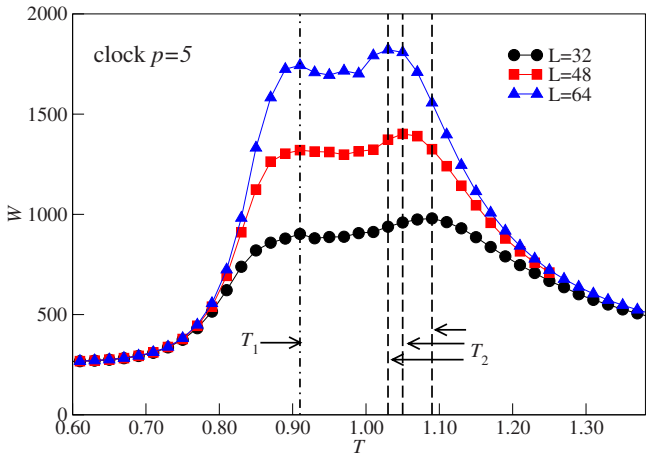

FIG. 12. (Color online) Roughness W as a function of the reduced temperature T for the $p=5$ clock model and several values of lattice size L. The simulation time is $t=2\times10^4$ MCS and the averages were taken over 2000 independent runs. The vertical dashed lines locate the transition temperature T_2, and the dot-dashed line locates the transition temperature T_1. The full lines are just guide to the eyes.

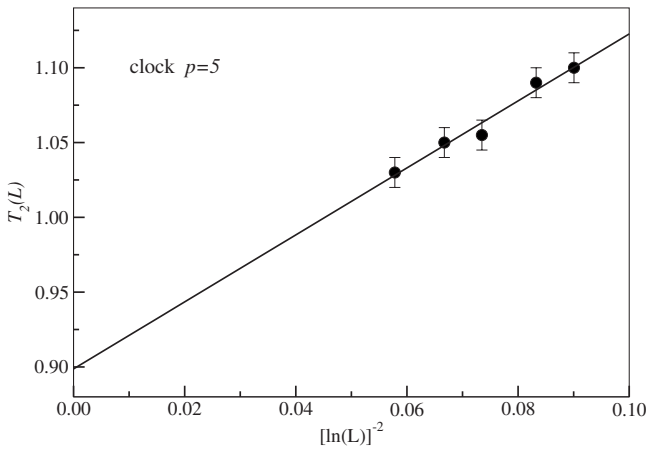

FIG. 13. Finite-size scaling of the temperature $T_2(L)$ obtained from the roughness W for the $p=5$ clock model. The line is the best fit according to Eq. (7).

4. Global phase diagram

Figure 14 shows the global phase diagram obtained from the above results in the reduced temperature versus number os states p plane. The transition temperature T_2 is of BKT type. However, the transition T_1 seems to have a different character than what happens from the disordered state to the spin-wave phase. As this transition has only a slightly size dependence we should argue that it can be first-order like. The surface exponent discussed below will give an extra indication of this behavior. In Fig. 14 the data for T_1 are the average of the results from the exponent β_w and from the roughness W.

V. GROWTH EXPONENT AND FAMILY-VICSEK SCALING

So far we were concerned only with the phase diagram of the model for general values of p. However, from a theoretical point of view, it is also important to determine the non-

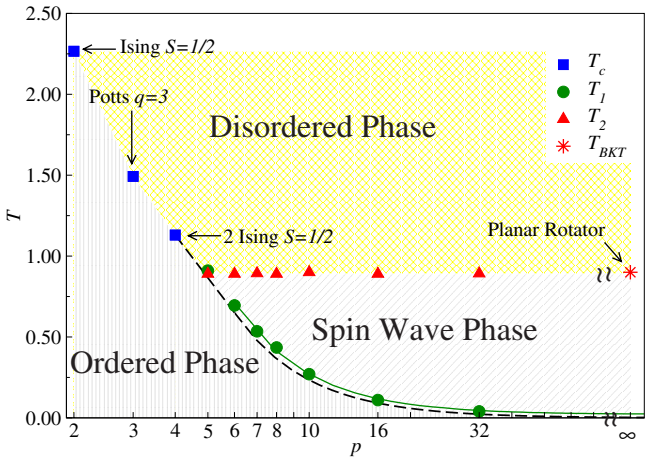

FIG. 14. (Color online) Phase diagram of the p-state clock model. The squares locate the critical temperatures T_c, the triangles the BKT transition temperatures $T_2=T_{BKT}$, and the circles the lower temperature transitions T_1. The errors are smaller than the symbol sizes. The full line is the best fit to a $1/p^2$ behavior and the dashed line is the corresponding T_1 transition line from Ref. [1].

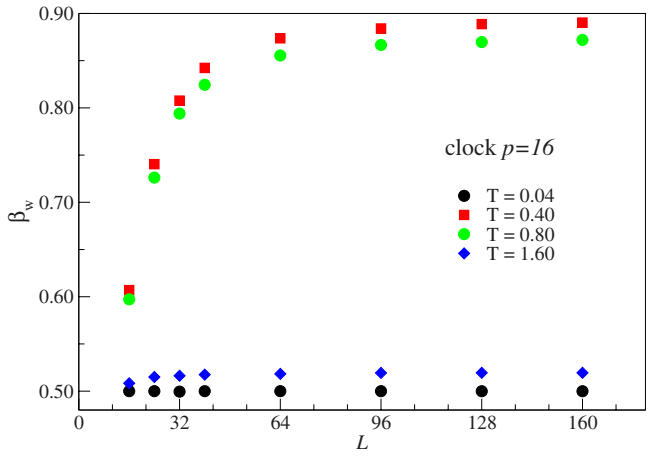

FIG. 15. (Color online) Growth exponent β_w as a function of the lattice size L for the $p=16$ clock model and several values of temperature. The simulation time is $t=200$ MCS and the averages were taken over 10^4 independent runs. The error bars are smaller than the symbol sizes.

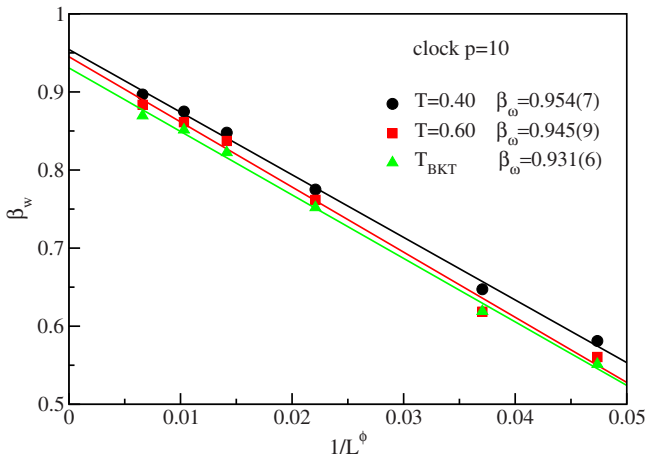

FIG. 16. (Color online) Growth exponent β_w as a function of the lattice size L for the $p=10$ clock model and several values of temperature. In this case one has $\phi=1.1$. The simulation time is $t=200$ MCS and the averages were taken over 10^4 independent runs. The error bars are smaller than the symbol sizes.

equilibrium surface grow exponents in order to characterize the corresponding universality classes for the present models.

Growth exponent

An inspection of Fig. 5 for the planar rotator model shows that the growth exponent β_w has a lattice size dependence. The same also happens for finite values of p (not shown). One can then compute this exponent for different values of the temperature. As a typical example we have in Fig. 15 the growth exponent as function of L for the $p=16$ states model and different temperatures. For temperatures below T_1 ($T=0.04$) and above T_2 ($T=1.6$) the exponent is close to 1/2, as expected because in these regions there is no correlation in the magnetic system. On the other side, for temperatures between T_1 and T_2 ($T=0.4$ and 0.8) the exponent is different from 1/2. Due to the lack of a finite size scaling for this exponent, we depict in Fig. 16 the best power law fits of this exponent for different temperatures for the $p=10$ model (with $\phi=1.1$). In this case we have $\beta_w^{p=10}(T=0.4)=0.954(7)$, $\beta_w^{p=10}(T=0.6)=0.945(9)$, and $\beta_w^{p=10}(T_{BKT})=0.931(6)$. For the planar rotator, a similar fit (with $\phi=0.8$) gives $\beta_w^{PR}(T_{BKT})=0.935(5)$.

Since the growth exponent β_w is calculated for short times, at the beginning of our simulations, we could expect a relation between this exponent and those obtained with the short time dynamics scaling (for a brief review see, for example [16]). In fact, for a second-order transition we obtained at T_c [8]

$$\beta_w = 1 - \frac{\beta}{\nu z} \quad (L \to \infty), \tag{8}$$

where β, ν, and z are, respectively, the order parameter ($m(T) \sim |T-T_c|^{\beta}$), correlation length ($\xi(T) \sim |T-T_c|^{-\nu}$) and dynamic critical ($\tau(L) \sim L^z$) exponents of the spin model. Here, starting from Eq. (2) and the scaling $m(t) \sim t^{-\eta/2z}$ at the BKT phase [17,18], we obtain

$$\beta_w = 1 - \frac{\eta}{2z} \quad (L \to \infty), \tag{9}$$

where η is the exponent of the correlation function spatial decay. For the planar rotator, for example, $\eta=0.238(4)$ and $z=1.96(3)$ [17] which gives $\beta_w^{PR}(T_{BKT}) \simeq 0.939$, in good agreement with the numeric result from our fit [$\beta_w^{PR}(T_{BKT})=0.935(5)$]. From Fig. 5 (for the planar rotator) and Eq. (9) (for the clock model) we can note also a slow decay of β_w with the temperature T at the BKT phase, which is in agreement with the increase in the value of the ratio $\eta/2z$ in this phase as we approach T_{BKT} [18,19]. In the next section, we will show that the dynamic critical exponent z can be obtained directly from the Family-Vicsek relation ($z=\alpha^*/\beta_w^*$). Thus, the exponents z and η can be obtained independently through this technique of mapping the spin configurations in a growth model.

Family-Vicsek scaling

It is well-known that the roughness W grows indefinitely as time increases, even at the second-order critical temperatures. As has been discussed in Ref. [8], this is related to the intrinsic noise in the Monte Carlo algorithms, where after the transients, the system follows a random walk in the phase space, adding a Gaussian noise to the temporal behavior of the mapped surface roughness W. This noise gives a diffusive factor in the thermal averages, resulting in the asymptotic $t^{1/2}$ behavior. This means that $\alpha \to \infty$ and that the Family-Vicsek scaling $z_w=\alpha/\beta_w$ is no longer valid. A way to extract the effect of the intrinsic noise from W, and to study the evolution of the roughness without this trivial growing, can be done by defining a roughness

$$W(\epsilon,t) = t^{1/2} W^*(\epsilon,t). \tag{10}$$

So, the noise-reduced roughness $W^*(\epsilon,t)$ should have a behavior similar to regular surface growing processes, scaling as $W^*(\epsilon, t \gg t_c) \sim \epsilon^{H^*}$, at short times as $W^*(t) \sim t^{\beta_w^*}$, and at

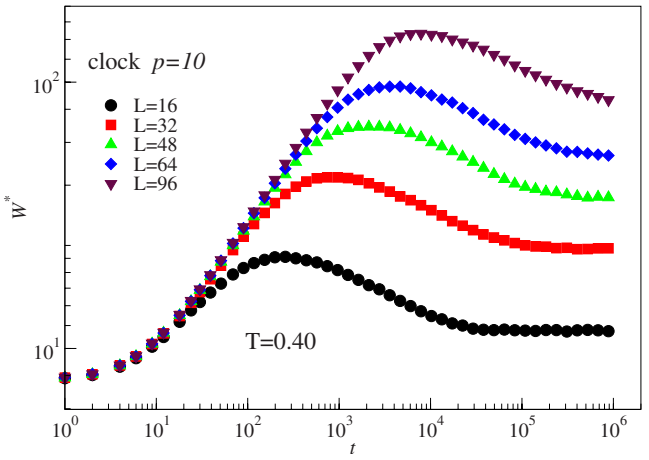

FIG. 17. (Color online) Log-log plot of the noise-reduced roughness W^* as a function of time t for the $p=10$ clock model at $T=0.4$ and several values of the lattice size L. The averages were taken over 10^3 independent runs to a maximum of 10^6 MCS. The error bars are smaller than the symbol sizes.

long times as $W^*(L,\infty) \sim L^{\alpha^*}$, where also $t_c \sim L^{z_w^*}$. We expect that $H^*=H$, $z_w^*=z_w$, $\beta_w^*=\beta_w-0.5$, and α^* can now be obtained through the behavior of $W^*(L,\infty)$ versus L.

Figures 17 and 18 show the noise-reduced roughness W^* as function of time for the clock model ($p=10$) and the planar rotator model ($p\to\infty$), respectively, at some temperature in the spin-wave phase and several linear lattice sizes L. One can see that the for the planar rotator model the roughness reaches its saturation in a steady way while for the clock model one has not only a maximum before the saturation, but also this saturation is achieved for one order of magnitude longer times than in the planar rotator case.

Figure 19 depicts the log-log plot of the saturation value of the noise-reduced roughness W^* where the slope gives us the exponent α^*. One has in this case $\alpha^{*PR}(T_{BKT})=0.875(4)$, $\alpha^{*PR}(T=0.6)=0.89(1)$, and $\alpha^{*p=10}(T=0.40)=0.88(1)$. From this we can show that the Family-Vicsek scaling ($z_w=\alpha/\beta_w$) holds for these cases: in fact, $z_w^*=z_w=\alpha^*/\beta_w^*$. For instance, for the planar rotator at T_{BKT} we have $\beta_w^*=0.935-0.5=0.435$ and $\alpha^*=0.875$, which gives $z_w=2.01$. For the $p=10$ clock model at T_{BKT}, $\beta_w^*=0.431$, $\alpha^*=0.86$, and $z_w=1.99(1)$. These results are comparable to the measured values of the dynamic critical exponent z for these models (we expect that $z=z_w=2$).

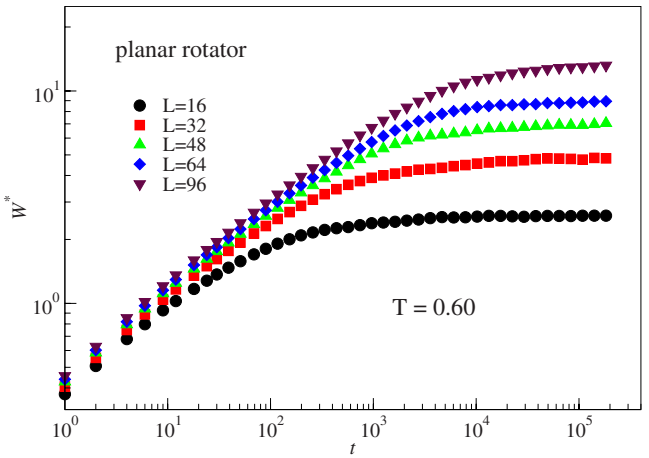

FIG. 18. (Color online) The same as Fig. 17 for the planar rotator model at $T=0.6$. The averages were taken over 10^3 independent runs to a maximum of 2×10^5 MCS. The error bars are smaller than the symbol sizes.

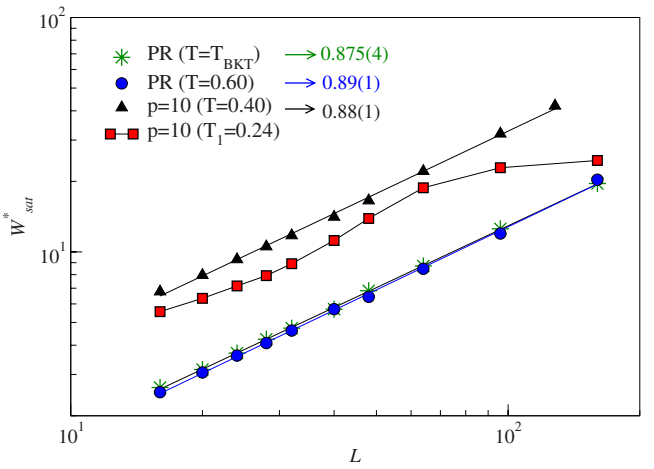

FIG. 19. (Color online) Log-log plot of the saturation values of the noise-reduced roughness W^* as a function of lattice size L for the PR and the $p=10$ clock model and several values of the temperature. The numbers give the slope of the curves which correspond to the exponent α^*. The averages were taken over 10–2000 independent runs to a maximum of 10^5-10^7 MCS. The error bars are smaller than the symbol sizes.

For the temperature T_1, on the other hand, we can see that the noise-reduced W^* saturates as a function of L, leading to an $\alpha^*=0$, which according to reference [8] is typical of a first-order character.

Finally, Figs. 20(a) and 20(b) show the data collapse of the results of Figs. 17 and 18, respectively. The values of the exponents α^* and z_w used in these collapses are fully consistent with the Family-Vicsek relation and the Eq. (9). The collapse for the $p=10$ clock model fails for short times because the system is still uncorrelated.

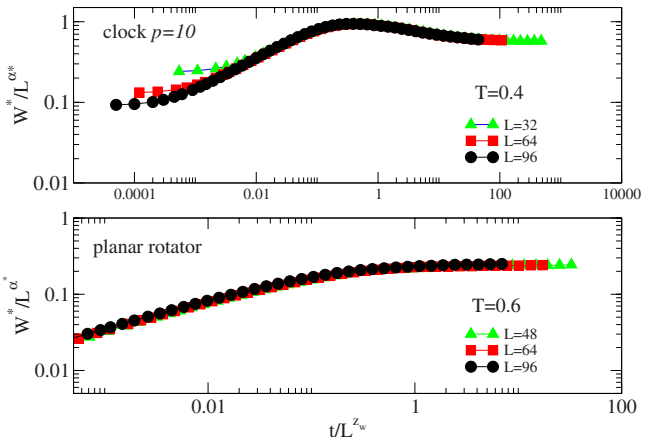

FIG. 20. (Color online) Log-log plot of the data collapse of the noise-reduced roughness W^*/L^{α^*} as a function of t/L^{z_w} for (a) the $p=10$ state clock model and (b) the planar rotator model.

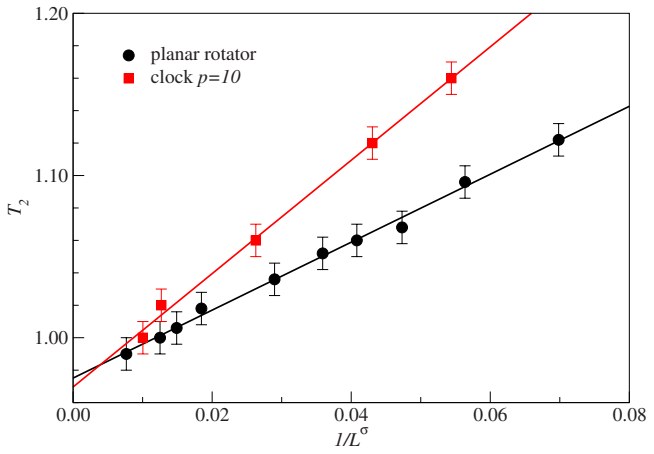

FIG. 21. (Color online) Finite size scaling of the temperature $T_2(L)$ for the planar rotator and $p=10$ clock model. The line is the best fit according to Eq. (11).

VI. CONCLUDING REMARKS

We have defined a growth model based on the dynamics of the discrete p-state clock model and also the continuous XY model (planar rotator). The phase transitions in these magnetic systems have been studied through the roughness technique. We were able to obtain the transition temperatures of the systems, static and dynamic exponents of the corresponding growing surfaces, as well as the characterization of the transitions. This dynamic approach for studying surface growth has shown to be adequate to treat not only discrete spinlike variables, but also continuous spin models, presenting the topological Berezinskii-Kosterlitz-Thouless transition. We argue that the present procedure would also be suitable to study continuous spin models presenting conventional second-order phase transitions, as well as multicritical phenomena.

The results for discrete finite values of p are also of the same quality as those for the Blume-Capel and Potts models previously studied. We should stress that in all the above analysis we assumed, from the beginning, that the scaling law for the XY universality class given by Eq. (7) is valid even for finite p. However, by considering a power law behavior

$$T_{BKT}(L) = T_{BKT} + \frac{C'}{L^{\sigma}}, \tag{11}$$

where σ is an additional exponent and C' a nonuniversal constant, our results for the high-temperature phase transition are qualitatively analogous to those presented above, with the only difference being the values of the T_2. As a matter of example, we show in Fig. 21 the transition temperature so obtained for the planar rotator model and $p=10$ clock model.

TABLE I. High and low transition temperatures T_2 and T_1 for the $p=6$ clock model obtained from the present procedure and compared with the results coming from different approaches. BKT stands for the XY-like behavior of Eq. (7) and power for the power law behavior Eq. (11). From Ref. [2] there are two measurements, one from the Fisher zero and other from the specific heat. T_1 from the present approach does not depend on BKT or power law behavior.

	T_1	T_2
Ref. [7]	0.6	1.3
Ref. [20]	0.68(2)	0.92(1)
Ref. [21]	0.68	0.90
Ref. [22]	0.7014(11)	0.9008(6)
Ref. [2] BKT—zero	0.74	0.88
Ref. [2] BKT—specific heat	0.79	0.86
Ref. [2] power—zero	0.632(2)	0.9997(2)
Ref. [2] power—specific heat	0.6068(1)	1.017(1)
Present work BKT	0.68(1)	0.90(1)
Present work power	0.68(1)	0.98(1)

In this case we have $T_2=0.975(2)$ and $\sigma=0.96$ for the planar rotator model and $T_2=0.970(4)$ and $\sigma=1.05$ for the $p=10$ clock model. It is interesting to notice that despite T_2 being different we get the same values (within the error bars) for all values of p. This situation has also been recently reported for the $p=6$ model where the Wang-Landau sampling has been used [2]. For comparison, we updated the table from Ref. [2] by including the present results (see Table I).

In addition, in treating the p-state clock model, we could get some insight regarding some unclear points on the global phase diagram. Apart from obtaining the extended universality in which not only the exponents, but also the critical temperature, are universal for $p>p_c$, we could show that within the surface approach the critical value for the number of states is $p_c=5$, since for this model one gets only one transition temperature. Moreover, the lower transition temperature T_1 seems to have a different character than the BKT transition occurring at a higher temperature T_2. In this case, at T_1 we find a strong indication of a first-order-like character.

ACKNOWLEDGMENTS

We thank the Brazilian agencies CNPq, CAPES, and FAPEMIG for financial support of this work. We thank also Albens P. F. Atman and J. G. Moreira for fruitful discussions.

[1] C. M. Lapilli, P. Pfeifer, and C. Wexler, Phys. Rev. Lett. **96**, 140603 (2006).
[2] C.-O. Hwang, Phys. Rev. E **80**, 042103 (2009).
[3] S. K. Baek, P. Minnhagen, H. Shima, and B. J. Kim, Phys. Rev. E **80**, 011133 (2009).
[4] V. L. Berezinzkii, Sov. Phys. JETP **32**, 493 (1971); J. M. Kosterlitz and D. J. Thouless, J. Phys. C **6**, 1181 (1973); J. M. Kosterlitz, *ibid.* **7**, 1046 (1974).
[5] S. Elitzur, R. B. Pearson, and J. Shigemitsu, Phys. Rev. D **19**, 3698 (1979).
[6] H. H. Roomany and H. W. Wyld, Phys. Rev. B **23**, 1357 (1981).
[7] J. Tobochnik, Phys. Rev. B **26**, 6201 (1982); **27**, 6972 (1983).
[8] A. F. Brito, J. A. Redinz, and J. A. Plascak, Phys. Rev. E **75**, 046106 (2007).
[9] A. L. Barabási and H. E. Stanley, *Fractal Concepts in Surface Growth* (Cambridge University Press, Cambridge, 1995).
[10] *Dynamics of Fractal Surfaces*, edited by F. Family and T. Vicsek (World Scientific, Singapore, 1991).
[11] P. Meakin, *Fractals, Scaling and Growth Far From Equilibrium* (Cambridge University Press, Cambridge, 1998).
[12] F. Family and T. Vicsék, J. Phys. A **18**, L75 (1985).
[13] P. Peczak and D. P. Landau, Phys. Rev. B **39**, 11932 (1989).
[14] D. P. Landau and K. Binder, *A Guide to Monte Carlo Simulations in Statistical Physics* (Cambridge University Press, Cambridge, England, 2000).
[15] W. J. Shugard, J. D. Weeks, and G. H. Gilmer, Phys. Rev. Lett. **41**, 1399 (1978).
[16] B. Zheng, Physica A **283**, 80 (2000).
[17] B. Zheng, M. Schulz, and S. Trimper, Phys. Rev. E **59**, R1351 (1999).
[18] P. Czerner and U. Ritschel, Phys. Rev. E **53**, 3333 (1996).
[19] X. W. Lei and B. Zheng, Phys. Rev. E **75**, 040104(R) (2007).
[20] M. S. S. Challa and D. P. Landau, Phys. Rev. B **33**, 437 (1986).
[21] A. Yamagata and I. Ono, J. Phys. A **24**, 265 (1991).
[22] Y. Tomita and Y. Okabe, Phys. Rev. B **65**, 184405 (2002).